High-Power Operation of a *K*-Band Second-Harmonic Gyroklystron

W. Lawson, H. W. Matthews, M. K. E. Lee, J. P. Calame, B. Hogan, J. Cheng, P. E. Latham, V. L. Granatstein, and M. Reiser

Laboratory for Plasma Research and Electrical Engineering Department, University of Maryland, College Park, Maryland 20742

(Received 1 April 1993)

Amplification studies of a two-cavity second-harmonic gyroklystron are reported. A magnetron injection gun produces a 440 kV, 200–245 A, 1 μs beam with an average perpendicular-to-parallel velocity ratio slightly less than 1. The TE_{011} input cavity is driven near 9.88 GHz and the TE_{021} output cavity resonates near 19.76 GHz. Peak powers exceeding 21 MW are achieved with an efficiency near 21% and a large signal gain above 25 dB. This performance represents the current state of the art for gyroklystrons in terms of the peak power normalized to the output wavelength squared.

PACS numbers: 85.10.Jz, 41.75.Ht

Linear colliders with a center-of-mass energy near 1 TeV would be of great interest in high energy physics research. To keep the length of such colliders within acceptable bounds, it has been proposed [1] to use accelerating gradients near 100 MV/m. Because the accelerating gradient is proportional to the product of the drive frequency and the square root of the pulse energy per unit length [2], this goal implies the use of high frequency microwave amplifiers with large values of output pulse energy. One scenario requires amplifiers with a frequency in the range 10–20 GHz, a peak output power near 100 MW, and a pulse duration near 1 μs. Because there are no sources that currently satisfy all these criteria, considerable research has been undertaken in the past few years to enhance the performance of existing amplifier technology. Configurations which are under investigation include conventional klystrons [3], relativistic klystrons [4], free-electron lasers [5], intense-beam traveling wave tubes [6], magnicons [7], CARMs (cyclotron auto-resonance masers) [8], and gyroklystrons [9].

Gyroklystrons combine the bunching mechanism of the cyclotron resonance maser (CRM) [10] and the ballistic bunching approach of the klystron. Overmoded cavities can be utilized because the beam-microwave interaction is coupled to the applied magnetic field through the cyclotron frequency and its harmonics. This facilitates the use of cavities with low electric fields and leads to the possibility of achieving higher peak powers. Another gyroklystron advantage results from the favorable scaling of the magnetron injection gun (MIG) with frequency [11]. Other benefits typically include gains (per cavity) and low-loss output waveguide modes.

Gyroklystrons have three potential drawbacks which can be avoided by careful design. The first is low efficiency, relative to klystrons, because gyrodevices tap energy primarily from the beam's perpendicular motion. This effect can be minimized by designing beams with high perpendicular-to-parallel velocity ratios ($\alpha = v_\perp / v_z$), by using short cavities, or by including energy recovery schemes [12]. The second obstacle comes from the free energy of the rotating beam, which can cause spurious CRM oscillations in various locations throughout the tube. This can be avoided by judicious loading of the drift tube with lossy dielectrics [13]. The final potential drawback is the large power required to supply the applied magnetic field. Actually, the required field strength of both high power gyroklystrons and klystrons for collider applications are similar [3,9]. This problem can be eliminated with superconducting magnets or alleviated by operating at a harmonic of the cyclotron frequency. The latter approach has additional advantages which are described below.

In recent years, our group at the University of Maryland has been investigating the properties of fundamental mode gyroklystrons with TE_{011} cavities. In a sequence of six two-cavity tubes, we have increased the state of the art [14,15] for these devices by $2\frac{1}{2}$ orders of magnitude by reaching powers near 24 MW at 9.87 GHz with efficiencies of 33% and gains in excess of 34 dB [16,17]. Two key steps in the process were the elimination of spurious oscillations and the optimization of the axial field profile. Subsequent three-cavity experiments [18] produced substantial increases in gain but only moderate power enhancement.

The cornerstone of our test bed where these results were produced is a 1 μs, 440 kV, 400 A line-type modulator which energizes a thermionic double-anode MIG [19]. The MIG produces a current up to 245 A; the rest of the current is shunted through a resistive divider which provides the voltage for the intermediate anode. An arrangement of eight water-cooled coils powered by four independent supplies allows for considerable flexibility in producing variations in the axial field profile. The design field in the circuit region is 0.565 T with a nominal magnetic compression of 12 occurring over a 0.4825 m distance. Computer simulations indicate that the velocity ratios typically achieved in the experiment are $\alpha \leq 1.0$. The corresponding axial velocity spread is in the (5–8)% range and depends on the beam current. A 2 μs, 100 kW, 9.7–10.0 GHz tunable magnetron provides the input power. Amplified power is axially extracted and travels through a nonlinear tapered wall section, the beam dump,

0031-9007/93/71(3)/456(4)$06.00

and a second tapered region to the half-wavelength output window. An anechoic chamber is used for preliminary stability and amplification studies and a directional coupler/liquid calorimeter system is used for high-power amplification measurements.

Our latest effort has been to evaluate the performance of second-harmonic gyroklystrons. To date, we have tested three different configurations. The advantages over fundamental systems include larger beam tunnels and output power (at a given frequency), lower capital costs, reduced power consumption and cooling requirements, and lighter weight. Potential disadvantages include increased opportunity for instabilities and reduced performance due to greater parameter sensitivity. One particular concern is that the rate of efficiency degradation due to velocity spread appears to be greater in harmonic devices.

The second harmonic tubes are derived from the fundamental devices by making a few changes. The same basic test bed is utilized with changes only to the nonlinear waveguide tapers (due to mode conversion considerations) and the microwave diagnostics. The new waveguide sections theoretically keep TE_{02} to TE_{01} mode conversion below -34 dB near the operating frequency. The anechoic chamber, which is used to estimate peak output power and mode purity, uses an open-ended section of K-band waveguide for the receiving antenna. Chamber coupling at the second TE_{02} maximum is -40.34 ± 0.25 dB at 19.75 GHz. The combination of a 20 dB directional coupler, variable precision attenuator, and a single-cavity bandpass filter provide an additional attenuation of 50.76 ± 0.15 dB. The detector diodes are calibrated against a power meter to ± 0.20 dB.

The calorimeter consists of a methanol load flowing between two conical polyethylene pieces in a 0.127 m diameter pipe. Designed for 10 GHz operation [9], the calorimeter load has a lower average dielectric constant and loss tangent at the second harmonic and experiences significant reflections at some frequencies. Nonetheless, it has proven adequate for the harmonic experiment. During calorimetry, a multihole mode-selective directional coupler is used to obtain the microwave envelope and an additional power estimate. The 0.127 m pipe doubles as the main arm and a cut down K-band waveguide acts as the secondary arm. The measured TE_{02} coupling at the operating frequency is -62.53 ± 0.50 dB. An additional attenuation of 28.88 ± 0.15 dB is provided by the auxiliary hardware described above (with a lower setting on the variable attenuator). A second directional coupler monitors TE_{01} activity near the fundamental frequency. The coupler is flooded with sulfur-hexaflouride to prevent breakdown.

The primary circuit modification is to replace the TE_{011}, 9.85 GHz output cavity with one that resonates in the TE_{021} mode at 19.70 GHz. The drift tube is also modified as described below. A schematic of the third microwave circuit is shown in Fig. 1. Two stainless steel tubes with standard knife-edged flanges brazed to the ends comprise the vacuum housing. The circuit is realized by stacking a series of metal and ceramic washers inside the housing. The main input cavity section has a length of 1.73 cm and a radius of 2.81 cm. The measured resonant frequency and quality factor are 9.84 ± 0.01 GHz and 380 ± 40, respectively. A thin carbon-impregnated aluminum-silicate (CIAS) ring located against the downstream end wall is used to load the cavity. The output cavity is machined from oxygen-free high-conductivity copper on a CNC (computer numerical control) lathe. The measured cold cavity resonant frequency and Q are 19.71 ± 0.02 GHz and 350 ± 25, respectively. The main cavity section has a length of 0.605 cm and a radius of 1.73 cm. The radius is selected to preclude fundamental amplification in the TE_{01} mode. Adiabatic wall transitions are used to minimize mode conversion to the TE_{01} at the second harmonic. The length is chosen to minimize the microwave signal flowing upstream toward the electron gun. The overall length of the cavity, including the integral output taper, is 9.42 cm. A scattering-matrix code [20] predicts the mode to be 99.4% pure and the power flowing upstream to be more than 38 dB down from the output power. A small-signal code predicts that the output cavity is stable at the desired operating point.

The preliminary drift tube is made mostly from CIAS rings. The main drift tube (between cavities) consists of nine tapered nonporous ceramic rings (80% BeO–20% SiC) surrounding a band-stop filter which is designed to prevent any 19.76 GHz, TE_{01} mode signal from propagating to the input cavity and electron gun. The maximum rejection is over 45 dB at 19.72 GHz and remains above 20 dB for more than 275 MHz. Attenuation in the TE_{11} mode (which is the most troublesome in fundamental mode tubes) is greater than 15 dB from 6.00 to 11.50 GHz. The total drift tube length is 12.28 cm and the minimum radius is 1.5 cm.

The search for the optimal operating point involves the systematic variation of beam voltage and current, drive frequency, magnetic field profile, and beam velocity ratio (via magnetic compression). As expected, the tube per-

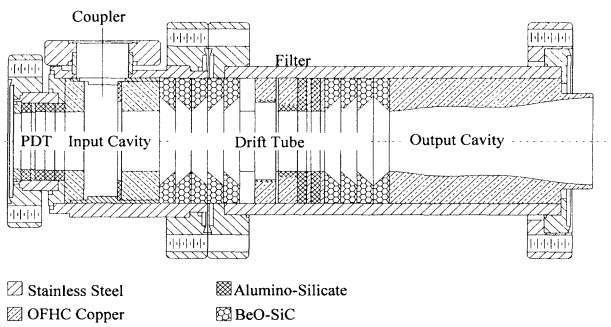

FIG. 1. The microwave circuit configuration.

formance is generally more sensitive to parameter variation than the fundamental devices. The second-harmonic tube is also more susceptible to instabilities and this limits its peak values of α to 1 or less. Two fairly benign spurious oscillations are often present at low levels during amplifier operation. The first is a gyrotwystron mode which produces a weakly amplified signal at the drive frequency in the output waveguide (after the final cavity). The second is a TE_{11}-like mode in the 6–7 GHz range that seems to interact with the beam in the drift tube and output cavity. The amplitude of this mode appears to decrease when output power in the desired mode is large.

At a given point in parameter space, we look for peak power by decreasing the cathode magnetic field (thereby increasing α) to a point just before the onset of an instability that degrades the amplified signal. The maximum power point is found when the beam voltage and current are 437 kV and 232 A, respectively. The drive signal is optimal at a frequency of 9.88 GHz and a power level near 60 kW. The optimum magnetic field is about 5.25 kG at the input cavity center and about 3% higher at the output cavity center. The peak power point is characterized by a strong interaction in the input cavity which is quite sensitive to the magnetic field.

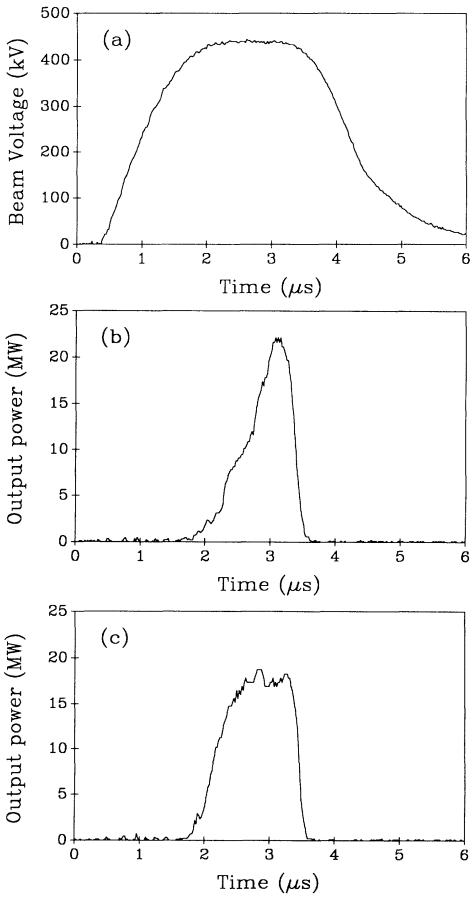

FIG. 2. Time evolution of the amplified signal at the optimal parameters: (a) the beam voltage, (b) the narrow pulse peak power, and (c) the broad pulse peak power.

The time dependence of the output power, unfolded from the detector diode, is shown for this point in Fig. 2(b). The corresponding voltage pulse is indicated in Fig. 2(a). The peak power of 21.6 MW corresponds to an efficiency near 21% and a gain over 25 dB. The narrow pulse width (20 MW is exceeded for only 250 ns) is due primarily to the time variation in α that results from a compensation problem with the resistive divider [17]. The pulse can be broadened at the expense of peak power by a slight adjustment of the magnetic feld. A typical shot of a 16 MW, 830 ns wide pulse (18.7 MW peak power) is shown in Fig. 2(c).

The far field mode pattern when the antenna is oriented to pick up the azimuthal electric field is indicated by the circles in Fig. 3. The theoretical pattern for a signal which is 0.7% TE_{01} and 99.3% TE_{02} is indicated by the solid line. This least-squares data fit is close to the cold cavity estimate discussed earlier. As to be expected with circular electric modes, a sweep of the far field pattern when the antenna is rotated by 90° picks up virtually no power.

The peak output power is shown in Fig. 4 as a function of beam current. The decrease at higher currents is presumably due to a dropoff in both beam quality and α, and a slight detuning with frequency. The microwave powers are comparable to (but less than) the fundamental two-cavity tubes even though the beam current is nearly 50% higher. Furthermore, the relative sensitivity of the output power to changes in beam current is over $2\frac{1}{2}$ times larger in the second-harmonic tube [9].

Similar results are obtained with the directional coupler/calorimeter assembly. This assembly changes the gyroklystron load sufficiently to modify the stable parameter space. Slightly higher powers are obtained at a current near 240 A and a moderately lower magnetic field in the input cavity. The calorimeter and coupler agree well near the peak powers, but their results diverge at lower powers due to the presence of spurious low frequency modes that are not seen by the directional

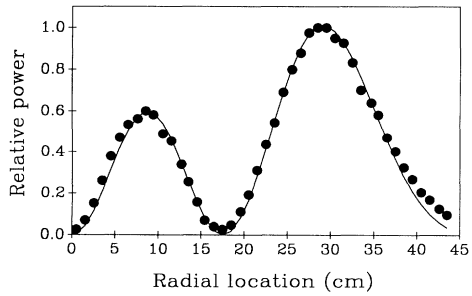

FIG. 3. Radial mode pattern of the anechoic chamber signal. The circles indicate the distribution of the amplifier output and the solid line represents the best theoretical fit (99.3% TE_{02}–0.7% TE_{01}).

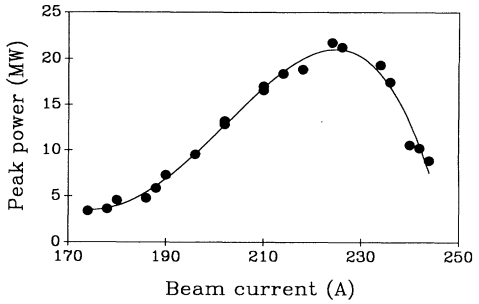

FIG. 4. Peak power measurement as a function of beam current. The other parameters are fixed at the optimal values.

coupler.

Attempts to simulate the operating point have been marginally successful. Our partially self-consistent large-signal code [21] does not predict the efficiencies obtained at the peak power levels (it is low by a factor of 2), nor does it confirm the sharp dependence on magnetic field. It does, however, predict the strong dependence on velocity ratio in that a 10% increase in α results in a doubling of the predicted efficiency. The disagreement between the simulations and experiment may be a result of the sensitive dependence on parameters coupled with the uncertainty in some of the beam quantities.

In summary, peak powers in excess of 21 MW have been produced in a two-cavity, 19.76 GHz, second-harmonic gyroklystron at an efficiency of 21% and a gain above 25 dB. This power level represents the state of the art for second-harmonic gyroklystrons. In terms of the ratio of peak power to output wavelength squared (an index derived from scaling laws), the relative power performance is over a factor of 3.5 times larger than the previous fundamental mode tubes and is comparable to the best results from klystrons [3]. A separate index based on accelerator requirements [22] also rates this tube near the state of the art. Considering the usual scaling laws, this tube could also be of interest in lower hybrid heating and radar applications.

Despite the less than optimal calorimeter, all three measurement schemes yield similar power estimates. This tube is more susceptible to instabilities than similar fundamental mode systems. It is possible that part of this problem originates in the resonant cavity of the band-stop filter. Since the mode content of the output cavity agrees well with theoretical predictions, it is likely that this trap is unnecessary. Another possibility is that the spurious modes originate in the relatively long output cavity. Future studies will look into the effect of trapless drift tubes and shorter output cavities and into the sensitivity of performance to the load requirements. Finally, work to improve agreement with theoretical efficiency calculations is under way and future tubes will incorporate capacitive probes to measure velocity ratio.

This work was supported by the U.S. Department of Energy.

[1] R. D. Ruth, in *Physics of Particle Accelerators,* edited by M. Month and M. Dienes, AIP Conf. Proc. No. 184 (AIP, New York, 1989), p. 2209.
[2] V. L. Granatstein and C. D. Striffler, in Proceedings of the Third International Workshop on Advanced Accelerator Concepts, Port Jefferson, NY, 14–20 June 1992 (to be published).
[3] A. Vlieks *et al.*, in *Proceedings of the 1991 Particle Accelerator Conference*, edited by L. Lizama and J. Chew (IEEE, New York, NY, 1991), p. 798.
[4] M. A. Allen *et al.*, Phys. Rev. Lett. **63**, 2472 (1989).
[5] T. J. Orzechowski *et al.*, Phys. Rev. Lett. **57**, 2172 (1986).
[6] D. Shiffler, J. A. Nation, and G. S. Kerslick, IEEE Trans. Plasma Sci. **18**, 546 (1990).
[7] M. M. Karliner *et al.*, Nucl. Instrum. Methods Phys. Res., Sect. A **269**, 459 (1988).
[8] W. L. Menninger *et al.*, in *Proceedings of the 1991 Particle Accelerator Conference* (Ref. [3]), p. 754.
[9] W. Lawson *et al.*, Phys. Rev. Lett. **67**, 520 (1991).
[10] J. Schneider, Phys. Rev. Lett. **2**, 504 (1959).
[11] W. Lawson, IEEE Trans. Plasma Sci. **16**, 290 (1988).
[12] M. E. Read *et al.*, IEEE Trans. Electron Dev. Pt. 2 **37**, 1579 (1990).
[13] J. P. Calame and W. Lawson, IEEE Trans. Electron Dev. **38**, 1538 (1991).
[14] A. C. McCurdy *et al.*, Phys. Rev. Lett. **57**, 2374 (1986).
[15] H. R. Jory *et al.*, in *International Electron Devices Meeting 1977 Technical Digest* (IEEE, New York, NY, 1977), p. 234.
[16] J. P. Calame *et al.*, J. Appl. Phys. **70**, 2423 (1991).
[17] W. Lawson *et al.*, IEEE Trans. Plasma Sci. **20**, 216 (1992).
[18] S. Tantawi *et al.*, IEEE Trans. Plasma Sci. **20**, 205 (1992).
[19] W. Lawson *et al.*, Int. J. Electron. **61**, 969 (1986).
[20] W. Lawson and P. E. Latham, IEEE Trans. Microwave Theory Tech. **40**, 1973 (1992).
[21] K. R. Chu *et al.*, IEEE Trans. Plasma Sci. **13**, 424 (1985).
[22] V. L. Granatstein and G. S. Nusinovich, in Proceedings of the 1993 Particle Accelerator Conference, Washington DC, 17–20 May 1993 (to be published).